

Nanostructured metallic foam electrodeposits on a nonconductive substrate

Woo-Sung Choi,^a Hye-Ran Jung,^a Se-Hun Kwon,^b Jong-Won Lee,^c Meilin Liu^d and Heon-Cheol Shin^{*ab}

Received 5th August 2011, Accepted 14th October 2011

DOI: 10.1039/c1jm13760c

A way to prepare the nanostructured metallic foam (NMF) electrodeposits on nonconductive materials was suggested for the first time. This innovative process involves the electrochemical preparation of NMFs on a metal-coated nonconductive substrate and subsequent removal of the deliberately heat-treated dense layer around the NMF trunks, leaving self-supported NMFs on the nonconductive substrate. The creation of nanostructured (or nanoramified) nickel foams on alumina was demonstrated as an exemplary application of the fabrication process.

1. Introduction

Nanostructured metallic foams (NMFs) may be used as a current collector or a support for electrodes or catalysts in chemical and energy transformation systems, including batteries, fuel cells, supercapacitors, solar cells, and reactors. The advantages of NMFs include excellent electrical conductivity, large surface area, high pore volume, and exceptional accessibility of active species to the internal surfaces for chemical, catalytic, and electro-catalytic reactions. The NMFs with properly tailored architectures may dramatically facilitate fast mass and charge transfer relevant to chemical and energy transformation processes. For example, self-supported nano-ramified foam structures, created by an electrochemical process, demonstrated enhanced performance of energy conversion devices.^{1,2} The most effective way to create NMFs is electrochemical deposition using gas bubbles as templates. This process has been studied by a number of researchers to explore its practical applications^{3–6} and further elucidate its formation mechanism.^{7–9}

Since a large electrical driving force must be applied to create ramified branches by dynamic templates of hydrogen bubbles vigorously generated in the deposition process, metallic foams have been constructed typically on metallic substrates (*e.g.*, copper) of high electronic conductivity and relatively low hydrogen over-voltage. The requirement of a metallic copper substrate, however, has severely limited the application of nano-ramified foam structures, which should be directly processed on electronically insulating electrolytes or semiconductors for many applications such as sensors and fuel cells. Although a thin film

of copper may be deposited on a nonconductive substrate and NMFs are subsequently created on the copper layer, the dense metallic film may act as a barrier to impede the normal function of the electrode.

Here, we report a way to fabricate the metallic foam structures with nano-ramified walls on a nonconductive substrate. In particular, any dense metallic layer or phase on the substrate will be completely removed so that the substrate surface will be either covered with NMFs or exposed to electrolyte solution, making it possible that the entire surfaces of the foam electrode are active and accessible to active species.

2. Experimental

An alumina plate was abraded with 100 grit SiC paper and cleaned with acetone before use as a non-conducting substrate. A dense copper layer was coated on the alumina plate by electroless deposition for 30 min (Incheon Chemical, ICP-360). The thickness of the deposited Cu layer was 350–400 nm. Ni–Cu foams were electrochemically deposited onto the Cu-coated alumina plate in an electrolyte composed of 0.4 M NiSO₄, 0.04 M CuSO₄, 1 M H₂SO₄ and 1 M NaCl. A platinum wire was used as the counter electrode and a constant current of 2 A cm⁻² was applied using an EG&G 263A. The sample was heat treated at 400 °C for 5 min under vacuum. After heat treatment, the electrochemical etching of Cu was performed in 0.5 M Na₂SO₄ solution using a three-electrode cell consisting of a Ni–Cu deposited substrate as the working electrode (anode), a platinum wire as the counter electrode (cathode) and a saturated calomel electrode (SCE) as the reference electrode. A constant potential of 0.2 V vs. SCE was applied until the measured cell current dropped below 0.5 mA.

The morphologies and chemical composition of the deposited films were analyzed using a scanning electron microscope (HITACHI S-4800 Field-Emission SEM, Japan) equipped with an energy-dispersive X-ray spectrometer (HORIBA 7593-H EMAX, Japan). A transmission electron microscope (FEI, Tecnai F30, The Netherlands) equipped with an energy-dispersive X-ray spectrometer (AMETEK, Genesis, USA) was used for the

^aSchool of Materials Science and Engineering, Pusan National University, Busan, 609-735, Korea. E-mail: hcshin@pusan.ac.kr

^bNational Core Research Center, Pusan National University, Busan, 609-735, Korea

^cFuel Cell Research Center, Korea Institute of Energy Research, Daejeon, 305-343, Korea

^dCenter for Innovative Fuel Cell and Battery Technologies, School of Materials Science and Engineering, Georgia Institute of Technology, Atlanta, GA, 30332-0245, USA

analysis of thin dense layers. For structural characterizations, the deposits were scratched from the substrate and the powder X-ray diffraction (XRD) pattern was recorded with an automated BRUKER D8 Advance diffractometer using Cu K α radiation.

3. Results and discussion

3.1. Conceptual model for creation of metallic foam on a nonconductive substrate

Shown in Fig. 1 is a simplified schematic description of the process for fabrication of metallic foams on a nonconductive substrate. Subsequent to the coating of a metal ($M1$, typically copper) on the nonconductive substrate for use as a current collector (step 1 in the figure), an $M2$ or $M2-Mx$ foam structure with a nanostructured wall is created on it (step 2). Then, the sample is heat-treated to form an $M1$ -rich alloy layer due to atomic diffusion between $M1$ and $M2(-Mx)$ (step 3). Subsequently, selective etching of $M1$ will completely remove the $M1$ -rich dense alloy layer on which there is virtually no foam structure (step 4), resulting in the $M2(-Mx)$ trees standing alone on the nonconductive substrate.

Three silent conditions for successful implementation of the fabrication process are as follows. First, the $M1$ and the $M2(-Mx)$ should form a solid solution with unlimited mutual solubility in the entire composition range to ensure complete

removal of the dense metallic layer. In the case where $M1$ and $M2(-Mx)$ form compounds instead of a solid solution, the formation of compound layer between the $M1$ and dense $M2(-Mx)$ phases could significantly slow down the atomic diffusion between them. Consequently, there is a strong possibility that a residual $M2(-Mx)$ dense film still remains even after prolonged heat treatment (in step 3); this would make the subsequent complete removal of the layer (in step 4) quite unlikely. Possible metal pairs for $M1$ and $M2$ are Cu–Ni, Cu–Au, Cu–Pd, Cu–Pt, Au–Ni, Co–Ni, etc.

Second, the thickness of the $M1$ coating and the heat treatment conditions should be such that all $M1$ phases in the $m1$ region of Fig. 1(d) are continuously inter-connected (*i.e.*, percolative) right after the heat treatment (in step 3), whereas the $M2$ phases are isolated from each other. In so doing, $M2$ can be effectively swept away when $M1$ is (electro-)chemically dissolved in step 4, leaving the bare surface of the nonconductive substrate open. To accomplish this, the thickness of the dense $M2(-Mx)$ deposits (a in Fig. 1(c)), on which there is virtually no ramified structure, should be pre-estimated in order to determine the minimum thickness of the $M1$ coating (b in Fig. 1(c)) and proper heat treatment conditions.

Third, the most important condition is that $M2(-Mx)$ should have a ramified or fractal growth habit under the deposition conditions. Here, Mx plays the role of modifying the growth pattern of $M2$ in order to achieve a highly ramified pattern, in the case where the electro-deposition of $M2$ hardly makes any ramified branches. If Mx is not beneficial to the subsequent process or the performance of the final metallic foam, it could be removed by subsequent (electro-)chemical etching. In this case, however, the volume fraction of $M2$ within the ramified deposits has to exceed that of Mx . Otherwise, $M2$ could be swept away during the course of Mx dissolution and the overall ramified structure may collapse.

On the other hand, an alternative method of exposing the bare surface of the nonconductive substrate is the use of a copper current collector on a partially masked substrate, followed by formation of foam just on the copper. However, the creation of a well-defined nanoporous foam structure is unlikely because vigorous hydrogen evolution is strongly suppressed on a partially inactive (or masked) surface. Furthermore, the production of masks is expensive and the process is difficult to scale to large areas. In contrast, our unique fabrication process will vigorously generate a sufficient amount of hydrogen gas bubbles as dynamic templates for the creation of a uniform and self-supported foam and is easy to scale up. At the same time, the pore size of the foam is proven to be readily controllable using an additive that is capable of lowering the hydrophobic force of the gas bubbles.¹⁰

3.2. Nanostructured nickel foam on an alumina substrate

To demonstrate the utility of this fabrication process, we created nickel foams with highly porous walls on an alumina substrate using the following steps: electrochemical deposition of nanostructured Ni–Cu ($M2-Mx$) foams on Cu ($M1$)-coated alumina substrates, formation of a Cu-rich dense alloy layer on alumina by heat treatment in vacuum, and final removal of the dense alloy layer.

It is well known that pure Ni has a layer-growth habit during the electrochemical deposition process.¹¹ However, it has

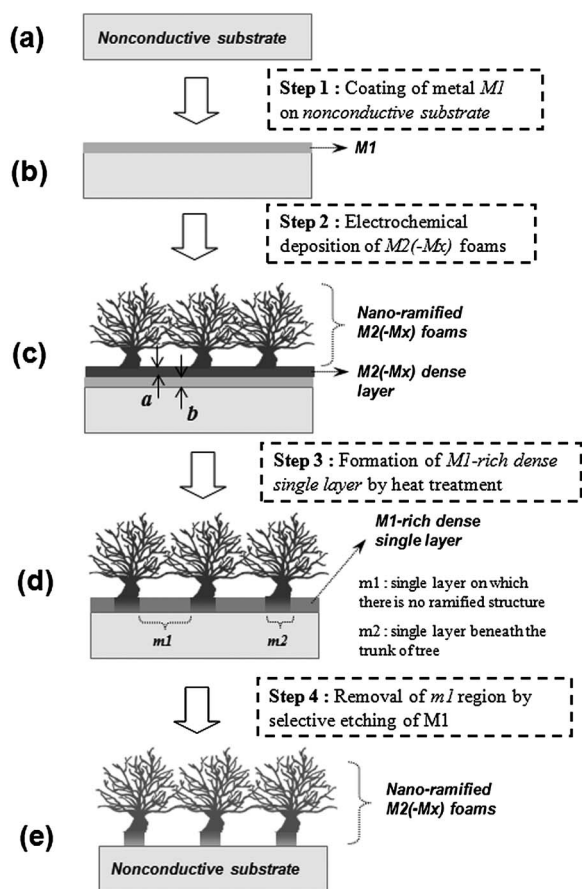


Fig. 1 Schematic illustration of the fabrication process of nanostructured metallic foams on a nonconductive substrate.

recently been reported that the co-deposition of Ni and Cu with chloride ions in the deposition bath considerably changes the growth tendency of the deposits so as to produce a nano-ramified structure,¹² due probably to the catalytic effect of the intermediate compound, CuCl.^{13–15} Under these circumstances, careful adjustment of the acidity (for hydrogen evolution) and the contents of nickel/copper/chloride ions (for the growth habit modification of Ni) allows successful creation of Ni–Cu foams with a nano-ramified structure, as shown in Fig. 2(a)–(d). The foam framework and nano-ramified walls are uniformly created throughout the deposits and the branch size ranges from several tens to hundreds of nanometres. The pores of the Ni–Cu foams are interconnected to a certain extent (please see the pores in the side walls of Fig. 2(b) and (d)). This interconnection comes from the random motion of the evolved hydrogen bubbles.

It is interesting to note that the proportion of Ni to Cu in the deposits decreases continuously in the direction away from the substrate (Fig. 2(c) and (e)). Although the cause of the gradient in atomic ratio is yet to be determined, it originates most likely from the faster consumption of Ni ions than Cu ions, due to the formation of an Ni-rich phase around the substrate, and the displacement of Ni by Cu in the deposition bath (*viz.* when we left the deposits in the electrolyte for a long time and then analyzed their composition, their outer surface proved to be pure Cu and CuCl₂). The higher content of Ni than that of Cu in the deposits

around the substrate enables the overall structure to survive even after the selective etching of Cu, because the Ni remains continuously connected in spite of the removal of the circumjacent Cu. On the other hand, it can be understood in the same context that the upper part of the deposits with a lower content of Ni than that of Cu collapses during the dissolution of Cu. This implies that there is a maximum thickness of the nano-ramified pure Ni structure that can be obtained under these conditions. Based on the compositional analysis (Fig. 2(c) and (e)), the maximum thickness to be survived after selective etching of Cu is estimated to be 10–15 μm , which is consistent with the experimental result (Fig. 6(d)). The maximum thickness is tunable by changing the electrolyte chemistry and thus the atomic ratio of Cu to Ni in the deposits.

The structural features of Ni–Cu foams are summarized for different periods of deposition in Fig. 2(f). It is noted that the average diameter of micron-sized pores on the surface increases with the foam thickness while their number decreases at a comparable rate, so that the foam wall becomes thicker. That is, the lower part of the deposit (*i.e.*, the part close to the substrate) has lots of micron-sized pores, while the upper part has a relatively large number of nanostructured branches or nanosized pores. This strongly indicates that the free volume which may facilitate the transport of active species becomes larger gradually as getting closer to the substrate and the electrochemically active area increases with the distance away from the substrate. This graded structure could be one of the most promising options for next generation functional electrochemical devices, where both a fast interfacial reaction and the facile transport of the active species play important roles in their performance.

Interestingly, the microstructure of the Ni–Cu foam is a little different from that of other metallic foams reported in our previous works,^{1,2,10} in view of the relatively non-uniform and thick foam walls. Although its origin is yet to be determined, the following three points are noteworthy: (1) the growth rate of the Ni–Cu foam is much lower than that of Cu or Sn foam. For example, the thickness of the Ni–Cu foam electrodeposited for 20 s (20 μm , please see the caption of Fig. 3) is only one-third of Cu foam (60 μm) and one-fifteenth of Sn foam (300 μm), deposited for the same deposition time.¹ It is quite likely that the lower deposition rate lets the energetic hydrogen bubbles more critically affect the microstructures of foams and in doing so the irregular motion of bubbles makes the wall structure more non-uniform. (2) The rate of increase in the foam thickness reduces with the deposition time, unlike the linear relationships between the foam thickness and deposition time, observed in the cases of Cu and Sn foam creation. This strongly indicates that the non-uniformity of the foam (wall) structure gets more remarkable due to the increased attack of the bubbles, as the foam is thickened. (3) The surface pore size of the Ni–Cu foam is much smaller than that of Cu or Sn foam with the same thickness. This means the hydrogen bubble size is smaller in the case of Ni–Cu foam. One possible reason for this is the difference in the surface where the bubble is generated: it formed on the Ni-rich dense film in this work (Fig. 4(a) and (b)) while it formed on the Cu in previous works.^{1,2,10} The different surface might lead to the different size of the initial bubble. The coalescence kinetics might be another potential reason for the different bubble size. Bubble coalescence

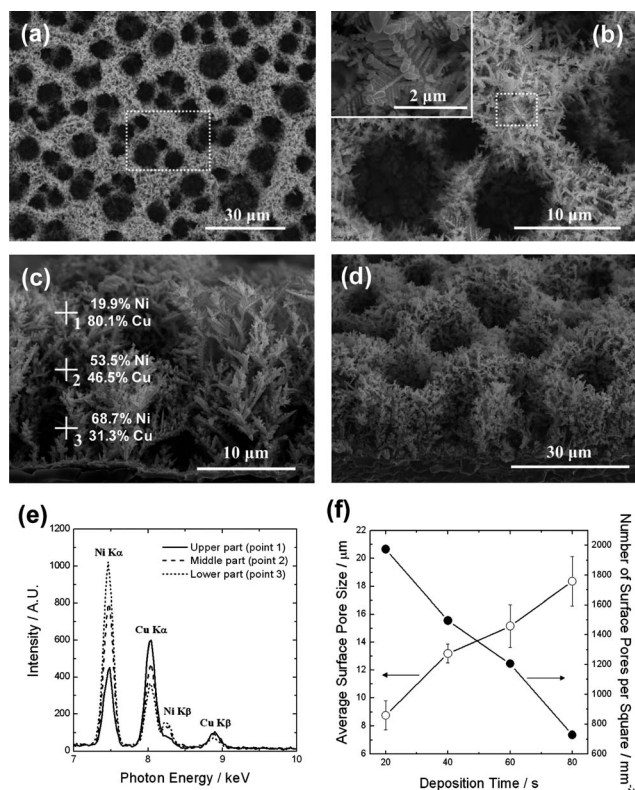


Fig. 2 (a and b) Top, (c) cross-sectional and (d) inclined views of nano-ramified Ni–Cu foams on an alumina substrate. (e) EDS spectra measured at different depths of nano-ramified Ni–Cu foams. The atomic percentages of Ni and Cu were determined therefrom and presented in (c). (f) Average surface pore size and surface pore density, estimated from Fig. 3.

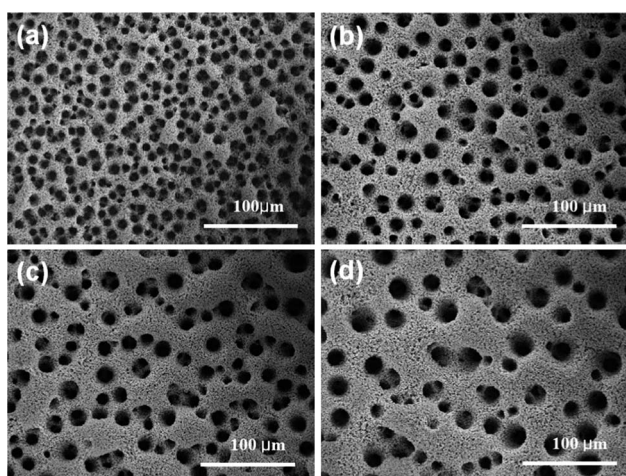


Fig. 3 Surface images of the Ni–Cu foam electrodeposits obtained for different periods of deposition time: (a) 20 s, (b) 40 s, (c) 60 s and (d) 80 s. The corresponding thicknesses of the deposits were estimated to be 20, 34, 46, and 57 μm , respectively, from the cross-sectional images (not presented in this work).

is closely related to the hydrophobic force of the bubbles, which is affected by the electrolyte chemistry.¹⁰ In spite of the above discussions, however, the origin of the difference in structural features among the metallic foams is still open to discussion.

From the experimental results presented above, it is confirmed that our Ni–Cu alloy satisfies the 3rd requirement for the formation of a metallic foam on a nonconductive substrate (*i.e.*, the ramified growth habit of the metal deposits M_2 – M_x). The first requirement is also fulfilled, because it is well-known that Ni and Cu form a continuous solid solution. To examine the second requirement (*i.e.*, the atomic continuity of metallic Cu after heat

treatment, in the m_1 region of Fig. 1(d)), the substrate/electroless Cu (b in Fig. 1(c))/electrolytic Ni–Cu dense layer (a in Fig. 1(c)) of the as-deposited sample was first analyzed. The average thickness of the electrolytic Ni–Cu dense layer and the atomic ratio of Ni to Cu of the layer, determined for the sample electro-deposited for 20 s, were estimated to be 50–100 nm and about 2.4, respectively (Fig. 4(a) and (b)). This implies that the selective etching of Cu of the as-deposited sample leaves a network of pure Ni, because the Ni atoms in the Ni-rich dense layer are interconnected with each other. The experimental confirmation of the above argument is presented in Fig. 5. The layer was not completely removed after selective Cu etching. Nano-sized holes in the image are most likely attributed to the dissolution of the Cu-rich region.

On the other hand, when the sample is subsequently heat treated, the Cu in the electroless Cu deposit (b in Fig. 1(c)) and Ni in the Ni–Cu dense deposit (a in Fig. 1(c)) diffuse into each other, to form a single Ni–Cu dense layer. Here, the thicker the electroless Cu layer, the lower the atomic ratio of Ni to Cu in the heat-treated single layer. From a rule of thumb calculation using the specific densities of crystalline Cu (8.92 g cm^{-3}) and Ni (8.91 g cm^{-3}), an electroless Cu layer with a thickness of more than 20–40 nm is needed to obtain a single dense layer with an atomic (or volumetric) ratio of Cu to Ni of less than 1.0 after heat treatment. Considering that the thickness of our electroless Cu is estimated to be 350–400 nm, the expected atomic (or volumetric) ratio of Ni to Cu is 0.084–0.185 in the single Ni–Cu layer after heat treatment.

Accordingly, based on the activation energy and the pre-exponential factor for inter-diffusion of Ni and Cu,¹⁶ the as-deposited sample was heat-treated at 400 °C for 5 minutes to make a Cu-rich single layer. It is noted that the interface between the electroless Cu and Ni–Cu dense layer disappeared and the atomic ratio of Cu to Ni was about 0.163 in the region where there has been no ramified structure (point 3 in Fig. 4(c)), which is consistent with our calculation. Now, it is expected that the Cu phase is inter-connected in a single layer, while the Ni phase or atoms are likely to be isolated by the Cu. This further implies that the isolated Ni could be physically swept away in the course of the selective etching of Cu, leaving the bare surface of the substrate open.

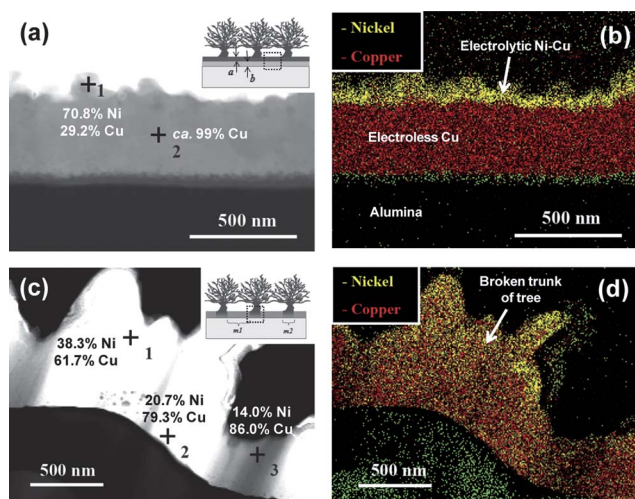


Fig. 4 Cross-sectional views (TEM images) and the corresponding atomic distributions of the dense layer on a nonconductive substrate, obtained from (a and b) the as-deposited and (c and d) the heat-treated samples. Insets in (a) and (c) show schematically the cross-sections indicating where the images were taken. The analyses were done for the samples where the trunk of the trees was mostly broken by ultra-sonication (*i.e.*, the point 1 of (c) is in the remaining trunk after sonication).

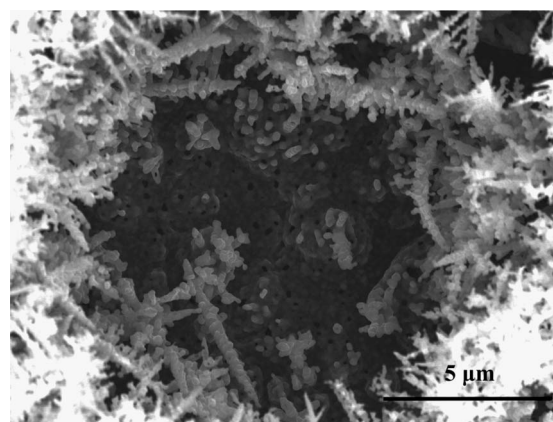


Fig. 5 Surface image of the electrolytic layer (a in Fig. 1(c)) observed after leaching Cu selectively from the as-deposited sample.

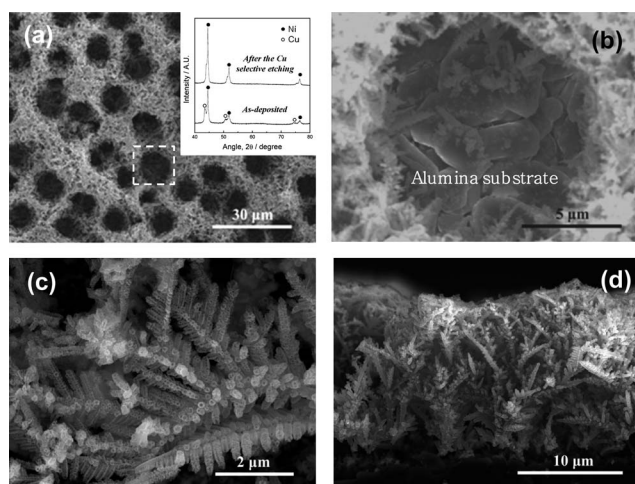


Fig. 6 (a and b) Top and (d) cross-sectional views of nano-ramified Ni foams on an alumina substrate after selective Cu etching of the heat-treated sample. (c) The magnified image of the branches. The inset in (a) shows X-ray diffraction patterns of the nano-ramified branches obtained from the as-deposited sample (bottom) and the sample subjected to heat treatment and subsequent selective Cu etching (top).

Shown in Fig. 6 are the microstructures of the deposits after the selective etching of Cu. While the overall foam structure was nearly identical to that of the as-deposited sample (Fig. 6(a) and (d)), two major differences were observed. One is that the dense deposits (*i.e.*, where there has been no ramified structure) disappeared, thereby causing the nonconductive substrate beneath them to be almost completely exposed, as observed in the surface view (Fig. 6(b)).

From the composition analysis, only aluminium and oxygen were detected on the exposed surface. It should be mentioned that the bottom of the trunk of the ramified deposits (*m2* in Fig. 1 (d)) has a lower Ni content which is similar to that of the dense deposits (*m1* in Fig. 1(d)), as indicated in Fig. 4(c) (see the composition at point 2), and might have been removed during the electrochemical etching. However, the contact area of *m2* to the chemical etchant is so narrow that its actual dissolution is negligible and, therefore, the overall foam structure is able to survive. The second is that the branch of the ramified deposits becomes translucent after the selective Cu etching (Fig. 6(c)). Cu removal out of the deposits is responsible for the porosity of the

branch and the transparency of the image. The X-ray diffraction pattern shows that the branch has only a trace amount of copper after chemical etching (inset of Fig. 6(a)).

4. Concluding remarks

A novel process for fabrication of 3-dimensional metallic foam structures on a nonconductive substrate has been demonstrated. Highly efficient electrodes based on the nanostructured metallic foams for solar cells and fuel cells are currently being investigated and will be reported in subsequent communications.

Acknowledgements

This research was supported by NCRC (National Core Research Center) program (2010-0001-226) and Converging Research Center program (2010K001091) through the National Research Foundation of Korea funded by the Ministry of Education, Science and Technology.

References

- H.-C. Shin, J. Dong and M. Liu, *Adv. Mater.*, 2003, **15**, 1610–1614.
- H.-C. Shin and M. Liu, *Adv. Funct. Mater.*, 2005, **15**, 582–586.
- Y. Li, Y.-Y. Song, C. Yang and X.-H. Xia, *Electrochem. Commun.*, 2007, **9**, 981–988.
- X.-Y. Fan, F.-S. Ke, G.-Z. Wei, L. Huang and S.-G. Sun, *J. Alloys Compd.*, 2009, **476**, 70–73.
- L. Trahey, J. T. Vaughey, H. H. Kung and M. M. Thackeray, *J. Electrochem. Soc.*, 2009, **156**, A385–A389.
- H.-R. Jung, E.-J. Kim, Y. J. Park and H.-C. Shin, *J. Power Sources*, 2011, **196**, 5122–5127.
- N. D. Nikolić, K. I. Popov, Lj. J. Pavlović and M. G. Pavlović, *J. Electroanal. Chem.*, 2006, **588**, 88–98.
- Y. Li, W.-Z. Jia, Y.-Y. Song and X.-H. Xia, *Chem. Mater.*, 2007, **19**, 5758–5764.
- J.-H. Kim, R.-H. Kim and H.-S. Kwon, *Electrochem. Commun.*, 2008, **10**, 1148–1151.
- H.-C. Shin and M. Liu, *Chem. Mater.*, 2004, **16**, 5460–5464.
- M. Paunovic and M. Schlesinger, *Fundamentals of Electrochemical Deposition*, Wiley-Interscience, London, 2nd edn, 1966.
- R. Qui, X. L. Zhang, R. Qiao, Y. Li, Y.-I. Kim and Y.-S. Kang, *Chem. Mater.*, 2007, **19**, 4174–4180.
- Z. Nagy, J. P. Blaudeau, N. C. Hung, L. A. Curtiss and D. J. Zurawski, *J. Electrochem. Soc.*, 1995, **142**, L87–L89.
- D. M. Soares, S. Wasle, K. G. Weil and K. Doblhofer, *J. Electroanal. Chem.*, 2002, **532**, 353–358.
- W. Shao and G. Zangari, *J. Phys. Chem. C*, 2009, **113**, 10097–10102.
- A. M. Abdul-Lettif, *Phys. B*, 2007, **388**, 107–111.